 DOI:10.48303/jsee.2019.241710

Technical Note

This is an extended version of the paper presented in SEE8 conference, peer-reviewed again and approved by the JSEE editorial board.

Seismic Response Evaluation of Kashan Historical Bazaar Structure Including Soil-Structure Interaction

Amirhossein Lazizi[1] and Hossein Tahghighi[2*]

1. M.Sc. Student, Civil Engineering Department, The University of Kashan, Kashan, Iran
2. Assistant Professor, Civil Engineering Department, The University of Kashan, Kashan, Iran,
* Corresponding Author; email: tahghighi@kashanu.ac.ir

Received: 15/04/2020
Accepted: 01/09/2020

ABSTRACT

Historical heritage structures are especially vulnerable to earthquakes because they were designed only for gravity loads without any consideration of lateral loads. For this reason, the preservation and maintenance of these structures are of great cultural, economic, and social importance. The present study investigates the seismic vulnerability of a historical structure called Kashan Bazaar, located in Kashan (central Iran), dating back to the 17th century. The detailed 3D geometrical model of this structure was drawn using SolidWorks software. Finite element numerical method was used to evaluate the response of Bazaar structure using macro-modeling approach. Static, modal, and nonlinear static (pushover) analyses were carried out using two cases, with soil-structure interaction (SSI) and without SSI (fixed-base). According to the results, considering the SSI has a significant influence on the mode shapes, vibration frequencies, and the structural responses. The structure of Bazaar can withstand gravity loads as well as DBE demands in fixed-base model. However, the results of the SSI analyses show the structure weakness against lateral loads.

Keywords:
Kashan historical Bazaar;
Finite element method;
Nonlinear static analysis;
Soil-structure interaction;
Seismic assessment

1. Introduction

Cultural heritage buildings represent a set of particular values, which are considered as every country's identity and history [1]. Today, the determination of the responsible institutes and the recommendations of the international councils on monuments and sites (ICOMOS) are to ensure the preservation of the identity and importance of these structures [2]. It is obvious that existing historic masonry buildings inherently have little capacity to withstand seismic loads, because in addition to low strength materials, horizontal load philosophy has been overlooked during their construction. Therefore, the performance of masonry structures against lateral load is ambiguous and needs further investigation. Due to the complexity of the geometry, material properties, and boundary conditions in historical structures, finite element method (FEM) is often used to assess their behavior [3-6].

Various approaches have been used for the seismic response analysis of masonry structures. Page [7] was one of the first researchers to consider numerical modeling of bricks. Lourenço et al. [8] modeled the masonry wall in a micro-level using contact elements. In this method, the masonry unit and mortar are defined separately. Due to the difficulty in understanding geometry, modeling, and the need for high computational effort, the micro-level analysis is suitable for small structures and structural details. Hence, there remains an important place for simple and practical numerical solutions to the analysis of large and complex engineering problems. The macro-behavior for

computational modeling of masonry structures was first proposed by Lourenço [9]. In macro-modeling method, a detailed description of the interaction between units and mortar is not necessary for seismic analyses on large structural members. From combined experimental and numerical results, it was concluded that macro-modeling technique may offer an adequate method to characterize the structural behavior [9].

Soil-structure interaction specially for structures resting on relatively soft soils amplifies the lateral displacements and influences the seismic performance and vulnerability of the structure [10-11]. Although for lightweight structures on stiff soils, ignoring the SSI effects might be acceptable, soft soil sites was found to have a significant influence on the force and displacement demands of foundation-structure system [12]. Therefore, in historical masonry structures due to the finite height and hard sections, the interaction between soil and structure could cause a serious impact. In the literature, there are very few studies for the seismic assessment of historical structures taking SSI into account. For example, Fathi et al. [4] computed the effect of SSI on the Tabriz historical Citadel using the concrete damage plasticity (CDP) model and macro-analysis. They reported that considering the SSI caused about 2.5 times increase in the vibration period, increased displacement, increased overturning probability, reduced acceleration and altered stress distribution. Güllü and Jaf [5] evaluated the historic masonry bridge by considering the SSI effect by means of complete three dimensional FEM. Their results showed that SSI can cause an increase in displacement by about 63% in the longitudinal direction and 80% in the transverse direction, as well as 12% decrease in acceleration along the longitudinal direction and 56% in the transverse direction.

In this paper, the seismic safety of the historical Bazaar in Kashan has been investigated. Following field surveys, a part of the Bazaar structure with minimal intervention and damage to the historic fabric of the structure was taken to create 3D geometrical model using SolidWorks program [13]. The ABAQUS finite element package [14] was used to perform the numerical macro-analyses. The results show that considering the SSI has a significant influence on the natural frequencies, modal shapes, seismic capacity, displacement demand, and the tensile damage distribution of the model. The structure of Bazaar can withstand gravity loads as well as DBE demand for the fixed-base condition. However, the analyses results with respect to the SSI effect show the structure weakness against lateral loads.

2. Kashan Historical Bazaar

The Bazaar in Pahlavi language has been used in the forms of Wazar and Vakar, which means a community or place to trade. The origin of this word in Iran and the world goes back several thousand years. The Bazaar first formed seasonally and then weekly in the vicinity of the large villages and became temporary from time to time. In order to utilize Bazaars in all seasons, ceilings were created for them and became permanent architectural structures. Kashan has been a place of cultural network since the ancient past, and its historical bazaar is one of the important commercial centers on the Silk Road [15]. The Kashan Bazaar complex has been registered as one of Iran's national monuments with registration number 1284. Figure (1) shows the location of Bazaar that includes more than 40 historical buildings in itself. This ancient complex has undergone many historical changes over the centuries. Its history dates back to the 10th century. The Kashan Bazaar suffered severe damage by a devastating seismic event occurred in December 1778 [16]. The present structure was rebuilt on the basement of the previous Bazaar.

Like other historical Bazaars of Iran that were created in the Islamic era, the Bazaar of Kashan has a linear structure and includes a series of interconnected masonry buildings implementing various functions. As shown in Figure (2), the Kashan historic Bazaar complex consists of a succession of vaults and consecutive arch that are 3 m to 5 m wide. Figure (3) shows the different components of the Bazaar. The main structure of the Bazaar includes a covered passageway with a large number of shops on both sides; its main pathway is called "Rasteh Bazaar". The Rasteh Bazaar has been constructed using Ribbed-vault (taq-va-cheshme). The Ribbed-vault system is one

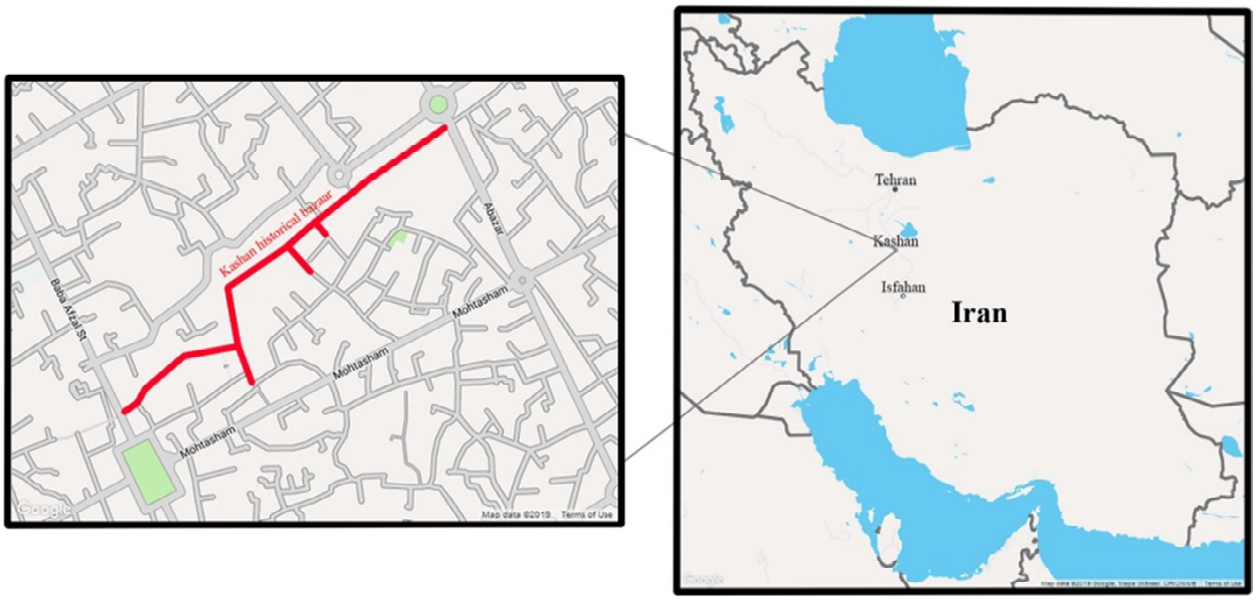

Figure 1. Location of Kashan Bazaar [17-18].

Figure 2. Kashan Bazaar path.

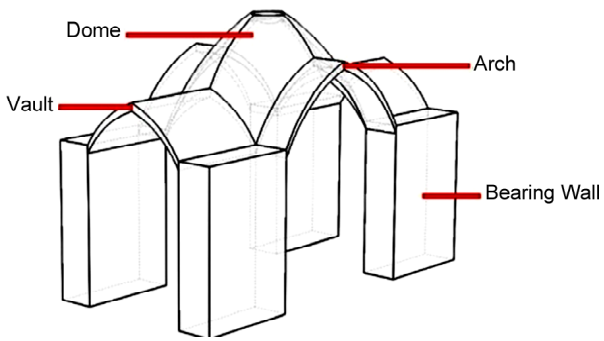

Figure 3. Components of Bazaar structure.

of the prominent Iranian methods of vault construction [15].

The Kashan Bazaar has suffered substantial damage during its life. The structural damages observed in the Bazaar are sometimes due to the lack of proper protection and maintenance or due to the possible loads and potentially damaging factors. Possible destructive factors consist of high gravity loads such as heavy snow or earthquake lateral loads. In some areas, the prevalence of these damages is such that the structural form of the bazaar has been altered. As shown in Figure (4), deep cracks can be seen in the arches of the Bazaar structure. Therefore, cracking through the gypsum board has not only distorted the beauty of the structure but has also altered the bearing performance of the structure. Note that, the selected segments for numerical modeling had no deep and severe cracks.

The permeation of moisture on the Bazaar arches, vaults and even domes is another observed damage in Kashan Bazaar. Generally speaking, there are two issues regarding moisture and masonry structure. The first is that moisture absorption by masonry is very high and the second is that moisture increases the rate of erosion of masonry. As a result, moisture is a major disadvantage for masonry. It should be mentioned that due to inadequate moisture insulation, lack of regular inspection and improper performance of the sewage system, the whole structure had high humidity (see Figure 5). Some

Figure 4. Deep cracks in the arches and vaults.

Figure 5. The permeation of moisture on the arches, vaults and domes.

Table 1. Mechanical properties of masonry [19].

Compressive Strength (MPa)	Tensile Strength (MPa)	Poisson Ratio	Elasticity Modulus (MPa)	Density (Kg/m^3)
2.4	0.12	0.2	1500	1800

adobe bearing pier walls were also out of their original form and were in poor condition. This inappropriate situation includes large cracks (even to the extent of coating removal), deformation, moisture permeation, and so on. Some of the domes of Kashan Bazaar structure have been executed flat after collapsing and during the repair. This contradicts the overall form of the Kashan Bazaar and has distorted the visual aesthetics of the structure. Thus, another point for finite element modeling was that the chosen segments were free from these tips (moisture, etc.).

3. Numerical Model

The studied historical Bazaar structure is composed of clay bricks and lime-cement mortar. The properties of masonry cannot be ascertained by the properties of the constituent materials and can only be obtained by experiment. Due to the lack of specific in situ testing and experimental data, the mechanical properties of the masonry material was assumed based on the LC1 knowledge level, provided by existing design codes [19]. Moreover, the implementation of a practical and straightforward model for the complex behavior of masonry material is still under investigation [20]. One of the main obstacles is the specificity of each masonry unit, which is in geometry and in the type of material. It was found that concrete damage plasticity based material model is suitable for the simulation of brittle materials such as ceramics and masonry [21-22]. Therefore, the CDP material model was used to perform numerical analysis. Table (1) illustrates the mechanical properties adopted for masonry in the present study. The parameters needed to define the CDP behavior model are given in Table (2).

Table 2. Plastic parameters of the CDP Model.

Eccentricity	Dilation Angle (°)	f_{b0}/f_{c0}	K_c	Viscosity (Pa-S)
0.1	10	1.16	0.67	0.002

Karimi et al. [23] performed a sensitivity analysis for the response of masonry structure to the plastic values of the CDP model.

The CDP model is based on the assumption of an isotropic damage description in tension and also in compression [14]. Figures (6a) to (6d) represent the masonry constitutive behavior in tension and compression. As shown in Figure (6a), the compressive stress-strain follows a linear relationship up to the yield stress, followed by a linear hardening up to the crushing stress. Then, a linear softening branch is assumed. However, the tensile stress-strain relationship is linear up to the peak stress, followed by a linear softening behavior (Figure 6b). For both tension and compression behavior, the decrease of the initial elasticity modulus is shown by two damage parameters of d_c and d_t using the following relationships:

$$\sigma_c = (1-d_c)E_0(\varepsilon_c - \varepsilon_c^{pl}) \quad (1)$$

$$\sigma_t = (1-d_t)E_0(\varepsilon_t - \varepsilon_t^{pl}) \quad (2)$$

where, σ_c is compressive stress, σ_t is tensile stress, E_0 is the initial modulus of elasticity, ε_c is the compressive strain, ε_t is the tensile strain, ε_c^{pl} is the plastic compressive strain, and ε_t^{pl} is the plastic tensile strain. The values of the damage parameters (d_c and d_t) vary between zero representing the start of softening and 1.0 at the end (Figures 6c to 6d). Since the employed tensile strength is noticeably lower than the compressive strength, only tension damage is assumed to be active.

The dilation angle controls the amount of plastic strain created during plastic shear. It is assumed that the dilation angle is constant during plastic failure. The degree of dilation angle in masonry is very low [22-23]. It is also not possible to extract this important parameter through testing. Eccentricity is related to the slope of the flow potential function. If it is considered zero, then the mentioned function would be linear; it also causes some difficulties to converge by very small values. f_{b0}/f_{c0} is the ratio of compressive strength of two-axis concrete to uniaxial compressive strength. For this parameter, a value between 1 and 1.27 is recommended [23]. There was a divergence in selecting values less than 1, but no change in values greater than 1.27. Viscosity is a parameter that helps to continue the solution after cracking and reducing hardness. Finally, for parameter K_c a value between 0.5 and 1 is recommended [23].

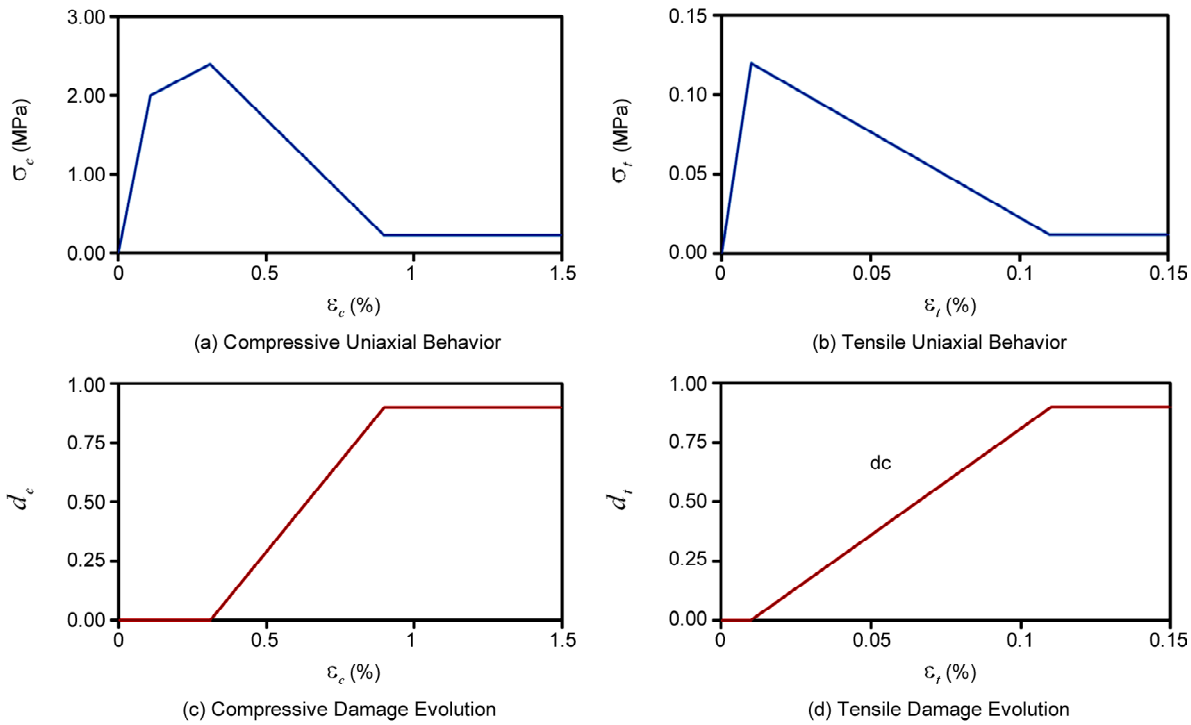

Figure 6. Masonry constitutive law in tension and compression used in this study.

Soil behavior is considered as elasto-plastic by Mohr-Coulomb constitutive model. The Mohr-Coulomb strength model is widely used in geotechnical issues. The validity of the results of the Mohr-Coulomb model has been verified by comparison with experimental results for sandy site soils [24-27]. In the Mohr-Coulomb behavioral model, failure is controlled by maximum shear stress, which is itself dependent on normal stress. In order to know the stress condition of the material at the moment of failure by the maximum and minimum principal stresses, Mohr circles must be drawn. According to Figure (7), the Mohr-Coulomb failure line is the best straight line to draw a tangent to these circles. The Mohr-Coulomb shear failure criterion is given by Equation (3).

$$\tau = c + \sigma \tan \phi \tag{3}$$

where τ is the shear stress, c is the material cohesion, σ is the normal stress, and ϕ is the friction angle of material. Table (3) shows the details of various soil properties, extracted from the actual geotechnical project [28].

In the numerical modeling process, geometric details play a key role. For this reason, two methods were used for more accuracy in collecting points. At first, the selected arches are captured from different distances, and then the images are analyzed using ImageJ software [29] and the different measures of sections are obtained. To ensure the validity of the software results, the size of different sections was also estimated using point transfer and triangulation method [30]. The values obtained in both methods overlapped well with each other. Finally, the geometric model of the Bazaar structure is constructed by SolidWorks software.

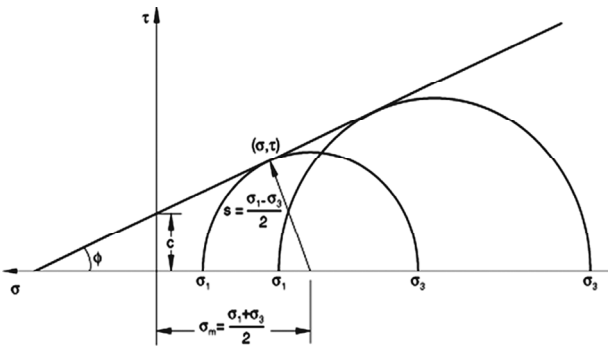

Figure 7. Mohr-Coulomb shear failure criterion [15].

The ABAQUS environment was used for structural analysis of the geometry imported from SolidWorks. The seismic assessment of Kashan historical Bazaar structure is studied with two comparative base conditions, the SSI and fixed-base systems. Figure (8) shows the detailed 3D finite element models with and without SSI. According to the previous research [31], the soil profile was assumed 45 m long and 21 m wide. Based on the geotechnical report [28], the sub-surface soil is considered as five layers and bedrock at a depth of 21 m. The interaction between the foundation and the surrounding soil was defined by contact elements using normal and tangential behavior. For this purpose, the coefficient of friction between the foundation and the surrounding soil was considered to be 0.577 [28]. The condition of stress continuity and deformation adaptation at the boundary between soil layers was considered by 9952 Tie elements in ABAQUS. 14382 and 9870 reduced brick octahedral elements (C3D8R) were used to meshing Bazaar structure and its foundation, respectively. Also, 32770 brick octahedral elements (C3D8) were used in order to soil meshing. Totally, 66974 elements and 91139 nodes were used in the numerical model to achieve realistic results. In order to apply the appropriate boundary conditions in the fixed-base model, the pier wall bases were fixed in all three translational directions. In the flexible base model, the degrees of freedom of the lateral sides of the soil profile were fixed in the case of

Table 3. Details of soil properties.

Layer No	Description	Thickness, T (m)	Density, γ_d (Kg/m^3)	Cohesion, C (Kg/cm^2)	Friction Angle, φ (Degree)	Moisture Ω (%)	Void Ratio, VR (%)	Poisson Ratio, υ	Elasticity Modulus, E (MPa)
1	Lean Clay	3	1650	0.07	30	13.46	19	0.33	25.77
2	Lean Clay	3	1360	0.1	36	17.35	29	0.34	29.12
3	Clayey Sand	2	1780	0.07	37	12.94	8	0.33	32.90
4	Lean Clay	10	1990	0.29	37	11.63	-	0.34	37.18
5	Lean Clay	2	1840	0.05	30	16.85	-	0.33	42.02

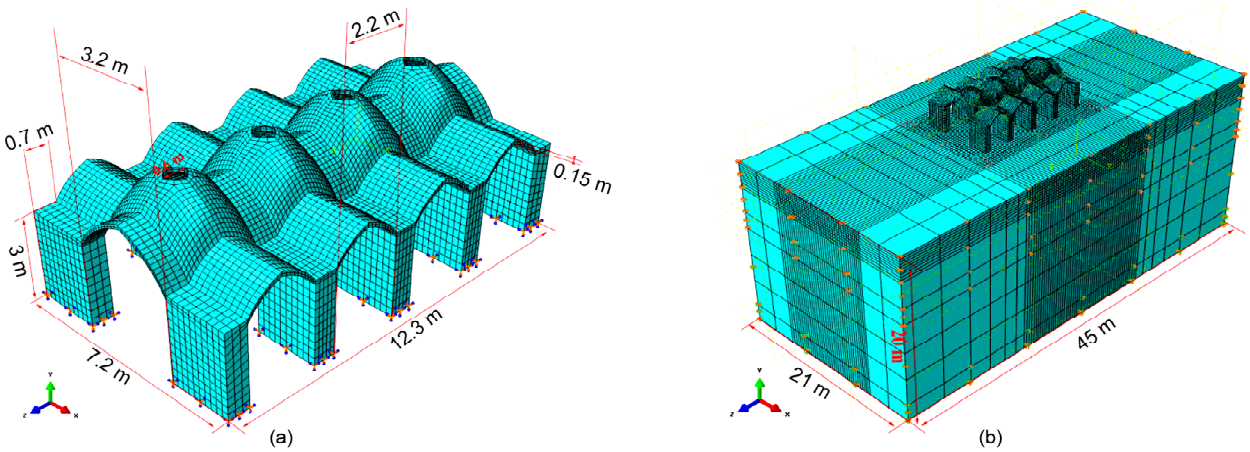

Figure 8. 3D view of the model and boundary conditions: (a) Without SSI, and (b) With SSI.

Table 4. Mechanical and geometrical properties of masonry wall [22].

Length (Mm)	Width (mm)	Height (mm)	Brick Size (mm)	Elasticity Modulus (MPa)	Poisson Ratio
1720	1500	195	195×195×45	7500	0.15

perpendicular to the plane. In order to simulate bedrock, the degrees of freedom of the soil profile were also fixed in all translational directions.

4. Validation of Numerical Model

The first step in numerical finite element modeling is to ensure that the workflow is correct. With the increasing use of numerical software and finite element modeling, coincidence (or closeness) of results to the reality is essential. Hence, model validation is performed to ensure the accuracy of numerical results. Karimi et al. [20] investigated the behavior of both masonry infilled and arch walls in a laboratorial manner. In order to validate the numerical modeling process of Bazaar structure, the wall tested in Ref. [22] was considered and the numerical results were compared with the experimental results. The masonry wall was constructed with solid brick clay and mortar plaster with a volume ratio of one to one. Also to obtain stress-strain diagram, uniaxial pressure test and three-point bending test was done [22]. Using the above information, the CDP model was used to model the masonry behavior.

It is noted that the reported plastic parameters by Ref. [22] were not valid values to define CDP model. After correspondence with the author of this Ref., the values of Table (2) were used for the present article. The geometry, boundary conditions, material properties and loads were modeled according to the laboratory sample. The masonry wall specifications are as shown in Table (4). Figure (9) shows the finite element model of the wall. In order to mesh the wall, the brick 10-node element (C3D10) and to mesh the U-shaped steel profiles, 4-node 3D rigid element (R3D4) was used, respectively. The analysis was defined as hysteresis and loading protocol similar to the experiment. Figure (10) compares the hysteresis curves obtained from numerical analysis and experimental data. Moreover, Figure (11) compares the envelope of hysteresis curves from the experimental and numerical analysis of the wall model. It is observed that the simulated results are in good agreement with the experimental measurements.

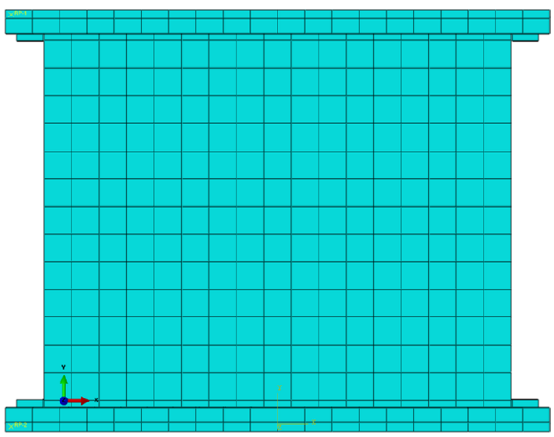

Figure 9. Wall numerical model.

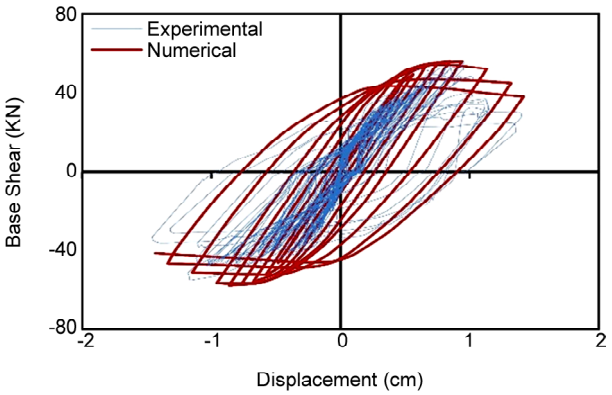

Figure 10. Comparison between experimental and numerical hysteresis curves.

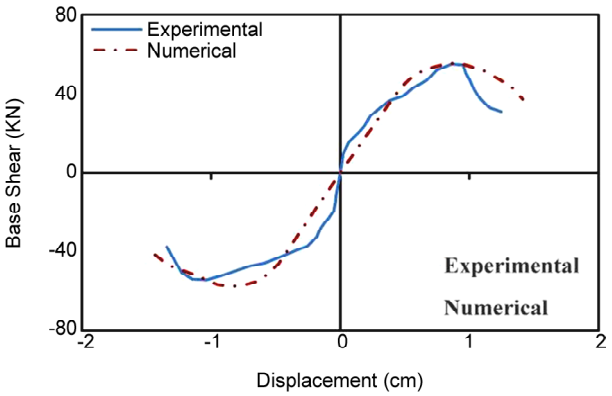

Figure 11. Comparison between experimental and numerical hysteresis curves envelope.

5. Numerical Analysis

After constructing the geometric model, defining the behavioral model, applying boundary conditions, and mesh generation it is necessary to show that numerical model can predict responses with acceptable accuracy and precision. The experimental frequency analysis is suitable to assess the accuracy of numerical modeling using the vibration characteristics of the system. Although the expression of vibration modes is a linear estimate, it can provide a good insight into the main weaknesses of the model. In addition, the vibration properties of the structure will be required in the nonlinear pushover analysis method. Therefore, modal analyses were performed on both 3D finite element models, with and without SSI, in order to define dynamic properties of the structure and its modal shapes. For eigenvalue analysis, there are three methods of AMS, Subspace, and Lanczos in ABAQUS software [14]. Due to the more capability of Lanczos in analyzing sophisticated issues, this method was used in the present study. Equation (4) gives the natural frequencies and modes of a system.

$$[K-\omega_i^2 M]\phi_i = 0 \tag{4}$$

where K is the stiffness matrix, ω_i is the ith eigenvalue (natural frequency), M is the mass matrix, and ϕ_i is the i^{th} eigenvector (natural modes).

Pushover procedure is frequently used for the seismic damage assessment. The seismic assessment of the structure is determined by a capacity curve. In which, the vertical axis represents the base shear and the horizontal axis indicates the displacement of the control point. Since the behavior of historical masonry throughout the structure is generally not the same, the choice of control point in the pushover analysis of such structures is crucial and vital. Therefore, it is better to use the mean of different control points at the same height instead of one control point [32-33]. In this study, the displacement control points are considered according to Figure (12). For pushover analysis, vertical loads including gravity loads are first considered. The lateral loads are then inserted separately in the positive and negative directions of the horizontal axes of the structure, namely X and Z in Figure (8). Note that due to the symmetry of the structural model, its response to lateral load in each coordinate axis has been investigated only in one direction. Lateral load distribution was assumed based on a mass proportional distribution proposed by NTC 2008 regulations [19]. The capacity curve was stopped at the corresponding displacement of the base shear equal to 85% of the maximum value [21].

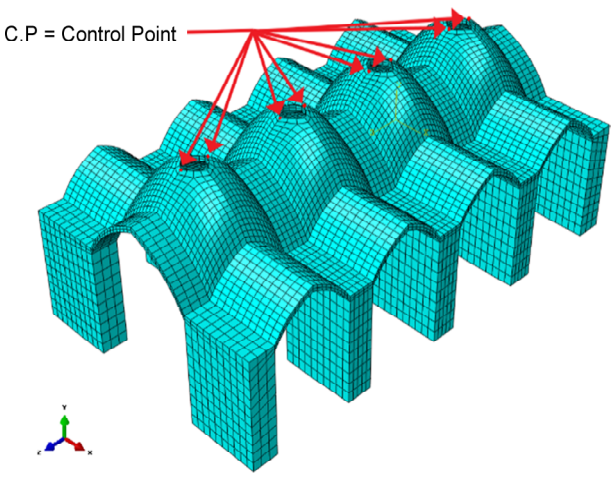

Figure 12. Displacement control points in the pushover analysis.

In order to overcome the complexity of numerical convergence, an implicit integration solver under quasi-static conditions has been used.

Structural vulnerability is investigated by using the N2 method [19]. In this method, using the participation factor, the multi-degree of freedom (MDOF) system is transformed into an equivalent single-degree of freedom (SDOF) system. Then based on the principle of equal energy, its capacity curve is transformed into a bilinear elastic-perfectly plastic load-displacement relationship. The elastic demand spectrum is then converted to an inelastic demand spectrum based on the equations given by Fajfar [34]. It should be noted that the elastic demand spectrum was extracted based on the Standard No. 2800 [35] for two earthquakes with a return period of 475 years (DBE) and 2475 Year (MCE). Then the capacity curve and the inelastic demand spectrum are taken to the acceleration-displacement response spectrum (ADRS) format. The point where the two curves collide is called target displacement.

6. Results and Discussion

The vibration period is an important parameter of a structure to estimate its seismic demand. Convergence analysis was performed to determine the most appropriate element size to be used in the finite element model. Table (5) shows the vibration periods of the first thirteen modes of the studied structure obtained in the modal analysis considering two comparative base conditions. The fundamental fixed-base period of the structure under study was evaluated as 0.101 sec, through the simplified formula of NTC 2008 (T_1 = 0.0187 h, height h = 5.4 m). As a consequence, the period value of 0.117 sec form numerical analysis (Table 5) is in agreement to the value provided by the NTC code. Furthermore, Table (5) provides the participation factors of the first thirteen modes for both the fixed-base and the SSI models. According to Table (5), the participation factors of the two base conditions differ in the same modes. It is observed that the important modes are displacement in both the first and fifth modes while the primary

Table 5. Vibration periods and participation factors for the first thirteen modes.

Mode	Base Condition	Period (sec)	Participation Factors				
			Trans X	Trans Z	Rot X	Rot Y	Rot Z
1	Fixed-base	0.117	0.00	1.43	4.03	5.14	0.00
	SSI	0.424	0.00	1.17	6.39	12.30	0.00
2	Fixed-base	0.096	0.00	0.00	0.50	0.00	0.29
	SSI	0.366	0.00	0.71	39.95	7.48	0.00
3	Fixed-base	0.076	0.21	0.00	0.00	1.28	0.93
	SSI	0.356	0.00	0.00	35.66	0.00	16.64
4	Fixed-base	0.076	0.00	0.00	0.00	0.66	0.00
	SSI	0.347	0.00	0.00	8.27	0.00	3.86
5	Fixed-base	0.074	0.00	0.18	0.94	0.65	0.00
	SSI	0.341	0.46	0.00	0.00	10.34	10.44
6	Fixed-base	0.071	0.30	0.00	0.00	1.87	1.21
	SSI	0.326	0.00	0.00	0.00	9.24	0.00
7	Fixed-base	0.069	0.00	0.00	0.00	11.5	0.00
	SSI	0.316	0.00	0.00	0.00	18.86	0.00
8	Fixed-base	0.065	0.00	0.00	0.57	0.00	0.33
	SSI	0.287	0.00	0.00	0.00	1.16	0.33
9	Fixed-base	0.064	0.00	0.00	0.00	3.18	0.00
	SSI	0.283	0.00	0.13	3.47	1.40	0.00
10	Fixed-base	0.061	0.00	0.00	0.51	0.31	0.00
	SSI	0.276	0.03	0.00	0.00	0.58	0.27
11	Fixed-base	0.060	2.35	0.00	0.00	14.43	7.06
	SSI	0.239	0.00	0.00	0.00	3.84	0.00
12	Fixed-base	0.048	0.00	0.00	0.55	0.18	0.00
	SSI	0.233	0.00	0.00	0.24	0.00	0.11
13	Fixed-base	0.047	0.00	0.00	0.18	0.00	0.10
	SSI	0.231	1.38	0.00	0.00	31.05	21.68

modes in terms of twisting for the fixed-base case are different than the SSI. Figure (13) shows a sensitivity analysis regarding the first mode vibration period of the structure and the number of elements used in the fixed-base model. The analysis indicates that when the number of elements increases, a convergent behavior is accomplished.

Figure (14) show the modal shapes of the Bazaar structure for the largest three vibration periods. According to Figure (14a), the first fixed-base mode is a combination of displacement in the Z-direction and rotation in the X-direction, the second mode rotation in the X-direction, and the third mode rotation in the Y and Z-direction. Regarding the reported results on Figure (14b), the first SSI mode is a combination of displacement in the Z-direction and rotation in the X-direction, the second mode rotation in the X-direction, the third mode rotation in the X-direction, and the displacement in the Y-direction. Therefore, we can conclude that considering SSI affects the modal shapes, so that by comparing the first 60 modes of the two base conditions only two common modes were found.

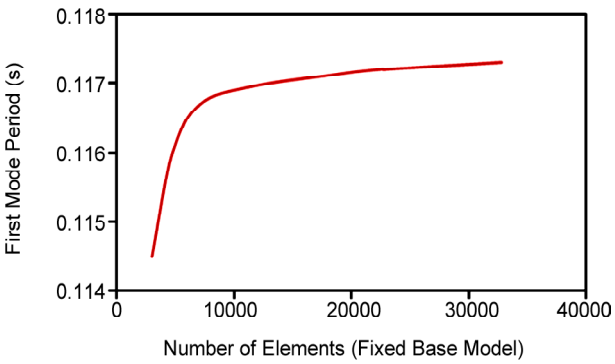

Figure 13. Fundamental vibration period versus number of finite elements for the fixed-base model.

The comparisons in terms of common modes are reported in Table (6), in which the vibration period in the SSI model is significantly higher than the fixed-base model. Seismic codes generally use the period ratio (flexible-base period, $\tilde{T}$ to fixed-base period, T) of structures to assess their response to earthquake loadings. As shown in Table (6), period ratio is ranging from 3.62 to 3.83 for the first two common modes. On the basis of FEMA 440 [35], the effective period ($\tilde{T}$) shall be determined as follows:

$$\frac{\tilde{T}}{T}=\sqrt{1+\frac{K^{*}_{fixed}}{k_x}+\frac{K^{*}_{fixed}h^2}{k_\theta}} \tag{5}$$

Table 6. Vibration periods of common modes of the models with different base conditions.

Mode	Base Condition	Period (sec)	Period Ratio
1	Fixed-Base	0.117	3.62
1	SSI	0.424	
11	Fixed-Base	0.060	3.83
13	SSI	0.231	

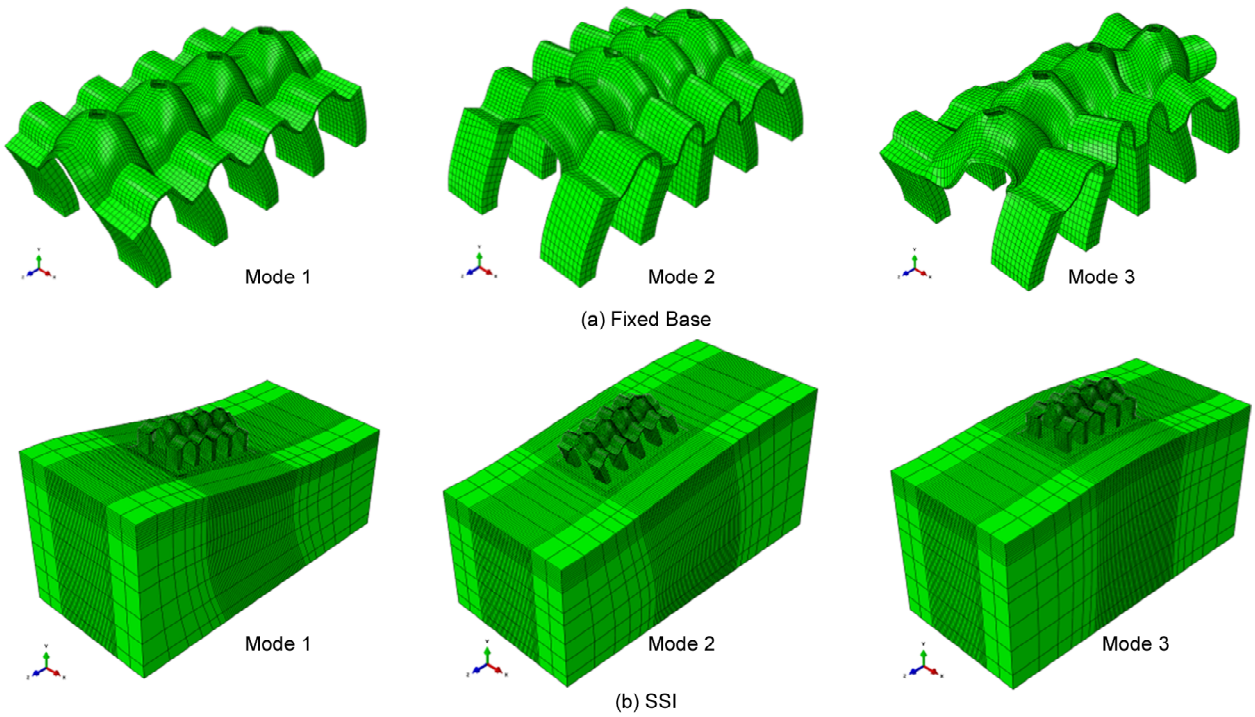

Figure 14. Modal shapes of the first three modes: (a) Fixed-base, and (b) SSI.

where K^*_{fixed} is the fixed-base model stiffness, h is the effective height of the structure, k_x is the horizontal stiffness of the foundation system, and k_θ is the rotational stiffness of the foundation. The soil properties are as presented in Table (3). Note that using the weighted average of the elastic modulus of different soil layers, the equivalent modulus of elasticity is assumed to be 34.32 MPa. The dimensions of the foundation were considered 14 m×9 m. Finally, the period ratio from Equation (5) is calculated to be 3.27. It can be seen that the effective period derived from the FEMA 440 guidelines is in good agreement with the results obtained by the numerical simulations.

Figure (15) shows the capacity curves of the studied models from pushover analysis. In order to describe the effect of the SSI, a comparison is presented between two different base conditions for fixed-base and SSI models. The reported results on Figure (15) show that the presence of the SSI in the system produces a decrease of initial stiffness and base shear, and an increase of displacement capacity. As shown in Figure (15), the SSI leads to a decrease of 9.6% and 4.4% in the base shear at the yield and collapse points, respectively, in the X-direction and also an increase of 233.3% and 294.1% in the displacement at the mentioned points. In addition, the base shear reduces as much as 32.2% and 23.6% for the yielding and collapse, respectively, and the corresponding displacements increase as much as 13.8% and 61.9% when the SSI is considered in the Z-direction. As expected, the SSI effect is more noticeable in the direction where the structure has higher stiffness. The differences in the overall flexibility of the models along the X and Z directions are associated to the presence of the bearing pier walls in the X-direction.

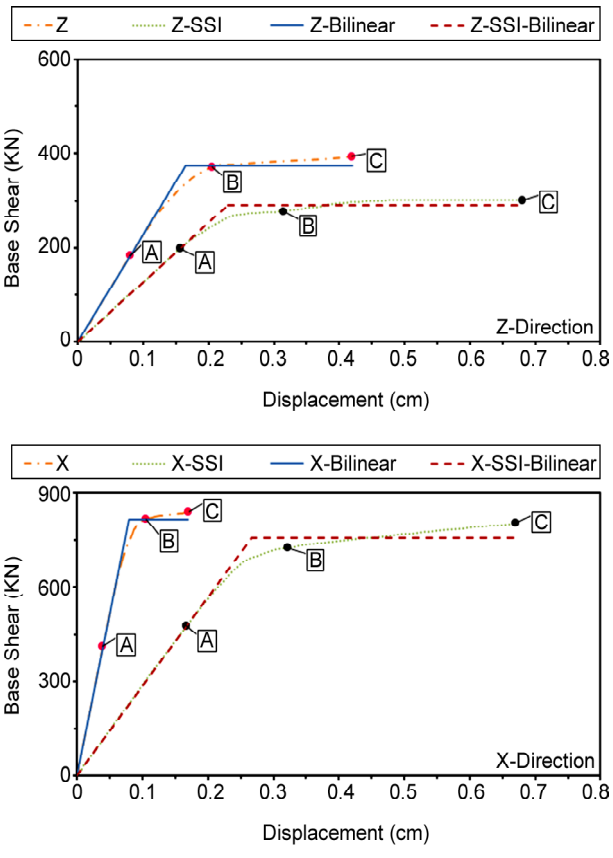

Figure 15. Comparison of capacity curves for fixed-base and SSI models (X and Z directions).

Figure (16) illustrates a comparison of pushover results between the capacity spectrum and the demand spectrum in the ADRS format. The bilinear capacity curve of the equivalent SDOF system is presented and the structural demands are for two different seismic intensity levels of DBE and MCE. Displacement demand and the displacement capacity arising from pushover analyses are compared to evaluate the seismic vulnerability of the structure. As shown in Figure (16), the fixed-base structure remains linear in the X-direction while moves to the collapse boundary in the Z-direction under the DBE demand. However, the results of SSI analyses for DBE demand led to the reduction of base shear, increase of displacement, and the reduction of safety factor due to the deformability of the soil. Although the structural capacity exceeds structural demand arising from the regulation spectrum along the X-direction, yet the structure does not have sufficient capacity in the Z-direction. Under the MCE demand, the structure will in no case withstand the resistance and will certainly collapse. Therefore, the obtained results show that the effect of SSI is detrimental to the seismic response of structure, and the neglect of SSI in analysis over-estimates the capacity of the structure and leads to unrealistic responses.

Figure (17) shows the contours of the damage prediction for different three time steps of the push over analysis (indicated by letters A, B, and C). These steps correspond to the occurrence of the ultimate tensile strain ε_{tu} = 0.15% (A), the onset of plastic yielding and the attainment of the ultimate strain in compression ε_{cu} = 1.5% (B), and the maximum displacement corresponding to the

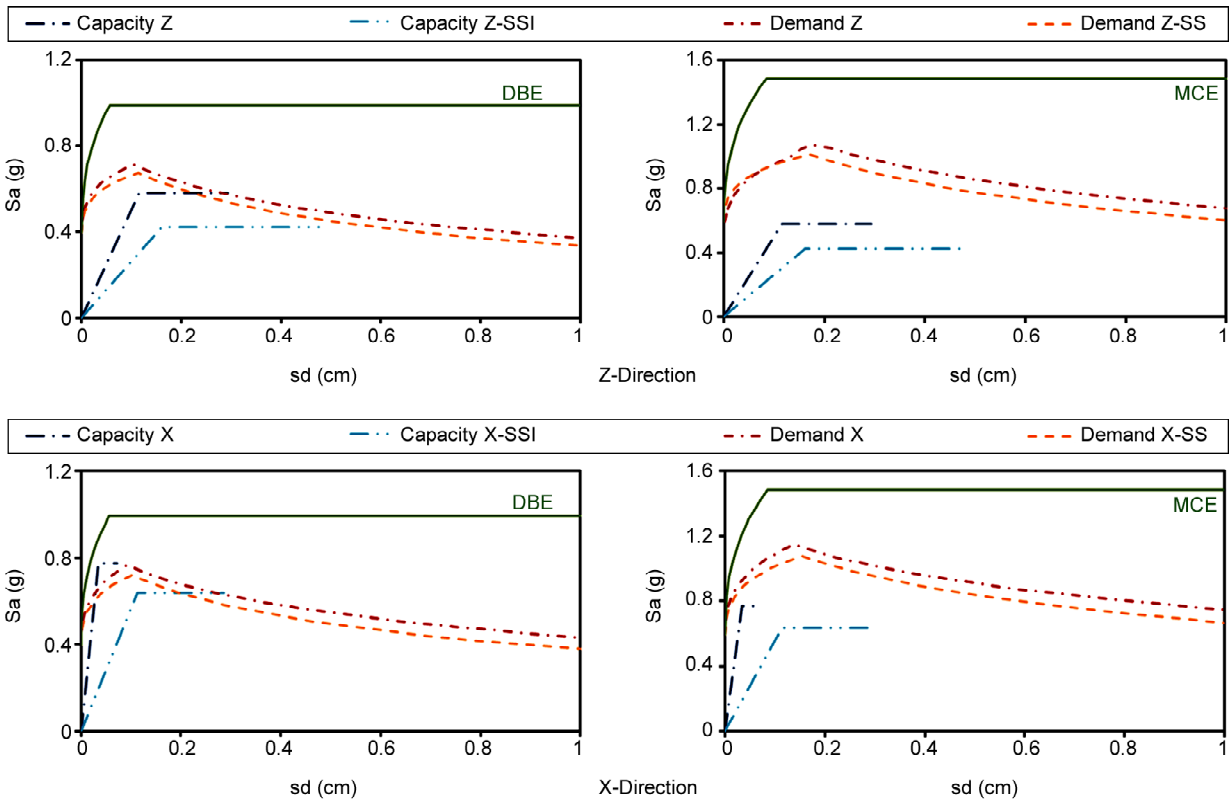

Figure 16. Comparison between capacity and demand spectra for fixed-base and SSI models in the ADRS format (X and Z directions) for different seismic intensity DBE and MCE levels.

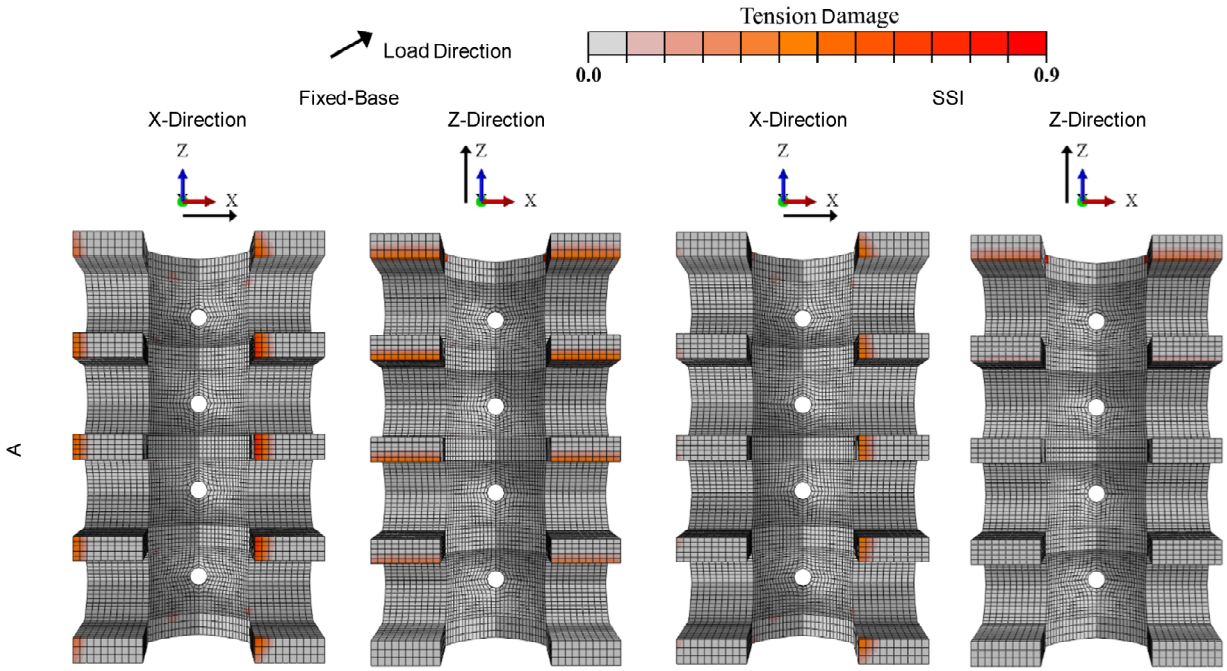

Figure 17. Damage distribution for fixed-base and SSI models (load direction: X and Z axes

collapse of the Bazaar structure (C). The reported results on Figure (17) are presented for both the fixed-base and the SSI models in X and Z directions. Even far from the structural collapse, the achievement of the ultimate tension strain is indicative of a local failure mechanism; thus it should be prevented in the case of heritage constructions. The analyses show that, in all cases, the onset of damage is associated with the occurrence of plastic yielding at the pier wall base. When the compression strain

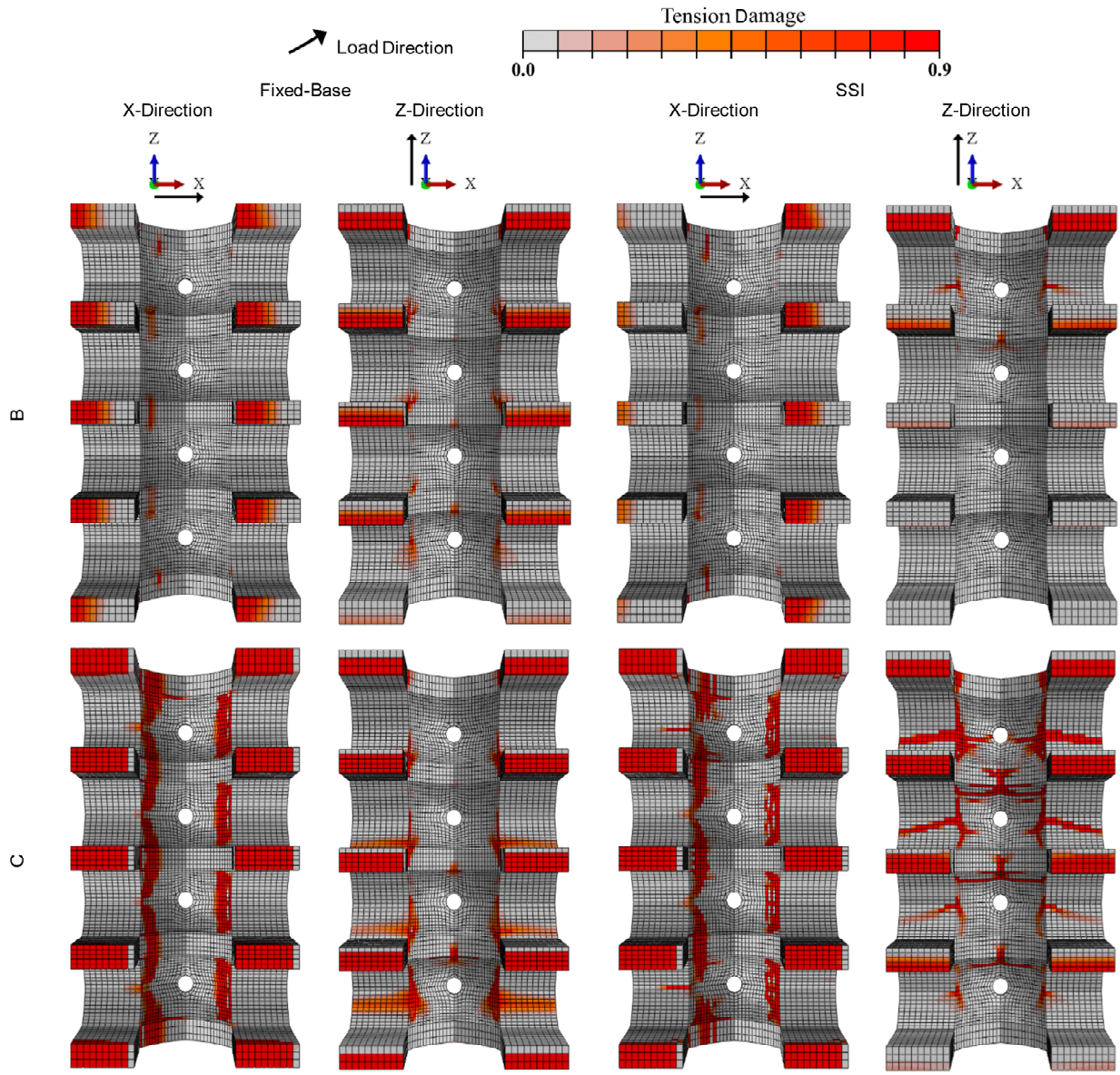

Figure 17. Continue.

exceeds its elastic limit, i.e. $\varepsilon_c = 0.3\%$, plastic points in the Z-direction tend to diffuse mostly in the upper regions including the dome-to-arch connection, the middle part of the short arches, and one-third of the pier wall side to the long arches. Moreover, in the X-direction, plastic points develop mainly at the dome-to-short and -long arch connection as well as the connection of short arch-to-adobe pier. It is observed that the structural damage, in the case of fixed-base model, is more widespread throughout the structure due to the rigid condition at the base. The analyses reported show that the damage configuration and plastic points basically alter with the effect of SSI. Hence, it can be concluded that the deformability of the soil has a considerable effect on the strain distribution and subsequently the damage contours.

Furthermore, the simulated results agree generally with those observed during the field surveys. Figure (18) shows the crack distribution by means of a representative photo taken from the survey compared with the obtained numerical results arising from point B of the push over analyses. It is observed that the typical seismic induced cracks are less marked than those of the numerical results. Note that such differences can be corresponded to the level of earthquake hazard assumed for the numerical simulation. As described in Section 5, seismic intensity was taken based on the design recipes of a current code [36], whose intensity level may differ with the actual level experienced during the structural life of the Bazaar.

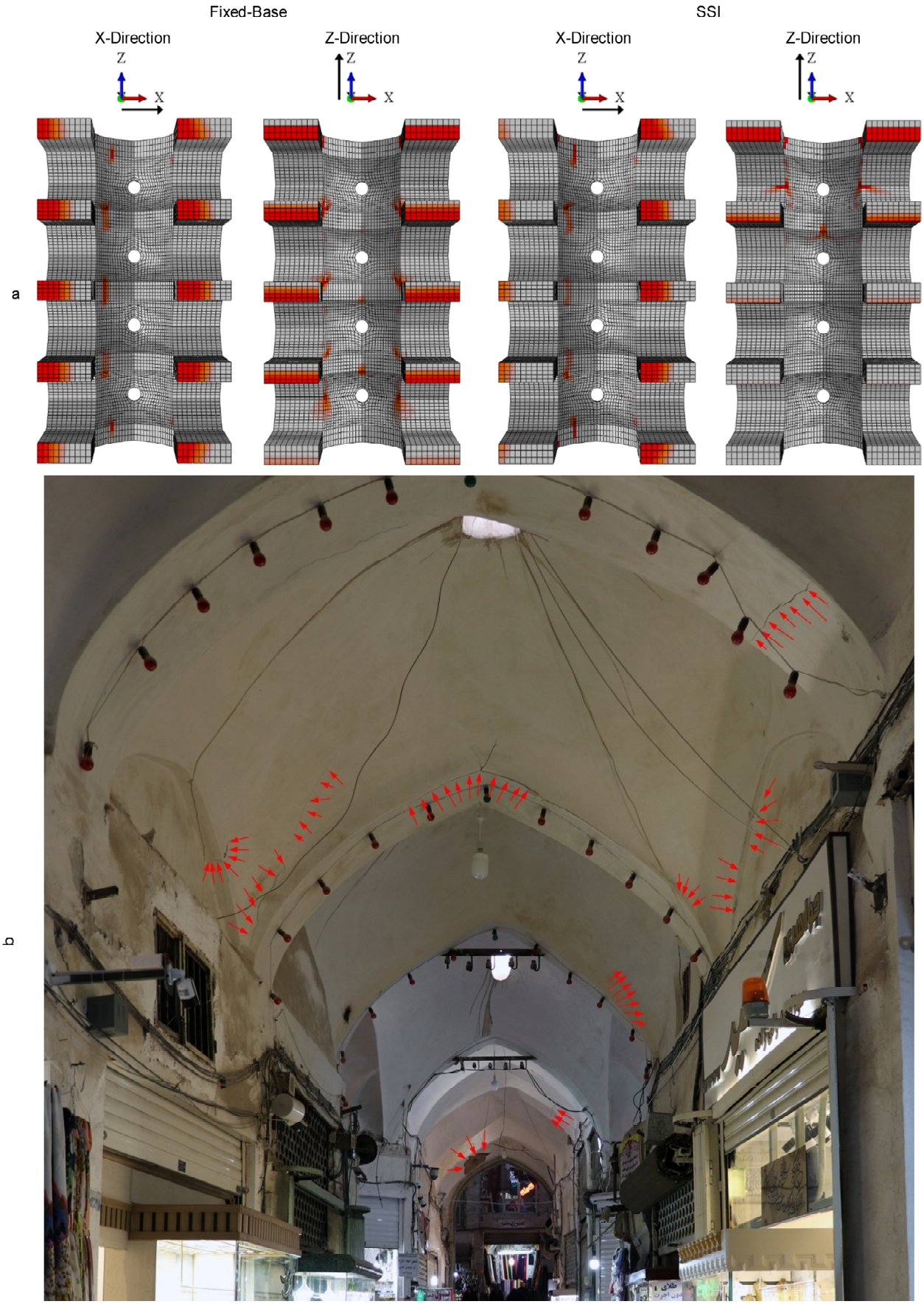

Figure 18. Crack distribution from: (a) Point B of the push over analyses, and (b) Representative photo of the survey.

7. Conclusions

The seismic vulnerability of Kashan historical Bazaar structure under the two hazard levels was assessed by three-dimensional pushover analyses with consideration of soil-structure interaction. The elasto-plastic behaviors of soil and masonry materials were modeled by the Mohr-Coulomb and CDP criteria, respectively. The numerical 3D finite element model of Bazaar structure was constructed in ABAQUS program. The accuracy of the finite element model was evaluated by comparing numerical results with the laboratory results. Based on the present research, concluding remarks are summarized as follows:

- Foundation flexibility has a significant effect on the vibration periods of the Bazaar structure. In fact, the SSI increased up to 3.62 times the fundamental period of the structure compared to the fixed-base condition.
- The comparison of capacity curves indicates that the lateral stiffness strengthened the SSI effect, since the overall flexibility of the system is more pronounced when the Bazaar structure is loaded along the direction with the presence of bearing pier wall.
- The Bazaar structure with the fixed-base condition exhibits a better performance than the SSI system. Accordingly, the effect of SSI is detrimental to the seismic response of structure and, therefore, the neglect of SSI in analysis leads to unrealistic responses.
- The Bazaar structure is able to sustain its stability against DBE demand for the fixed-base condition. However, the weakness of the structure is observed to increase when SSI effects are incorporated. It will also collapse due to the MCE demand intensity.
- The structural damage distribution and plastic points were basically affected by the flexibility of foundation. Moreover, damage configurations from numerical analyses are in a general agreement with those of the survey.

Finally, the results obtained in this article can be helpful to quantify the SSI effects on the seismic assessment of a historical construction. However, this study still needs to be verified for additional more-time consuming nonlinear dynamic simulations to show more accurately the high vulnerability of ancient masonry structures due to horizontal loads. Consequently, consistent ground motions that have similar mechanism to the nearby faults should be adopted to reproduce seismic loads. Furthermore, the mechanical parameter for the constitutive model can be improved using field experimental data. This information will be definitely essential for seismic retrofitting decision-making process of such structures.

References

1. Feilden, B. (2018) *Conservation of Historic Buildings*. Routledge, 4th edition, London.
2. ICOMOS Recommendations (2005) *Recommendation for the Analysis, Conservation and Structural Restoration of Architectural Heritage*. International council on monument and sites, Barcelona.
3. Silva, L.C., Mendes, N., Lourenço, P.B., and Ingham, J. (2018) *Seismic Structural Assessment of the Christchurch Catholic Basilica*. New Zealand. Structures, 15, 115-130.
4. Fathi, A., Sadeghi, A., Azadi, M.R.E., and Hoveidaie, N. (2019) Assessing seismic behavior of a masonry historic building considering soil-foundation-structure interaction (Cases study of Arge-Tabriz). *International Journal of Architectural Heritage*, 1-16.
5. Güllü, H. and Jaf, H.S. (2016) Full 3D nonlinear time history analysis of dynamic soil-structure interaction for a historical masonry arch bridge. *Environmental Earth Sciences*, **75**(21), 1421. DOI:10.1007/s12665-016-6230-0.
6. Pena, F., Lourenço, P.B., Mendes, N., and Oliveira, D.V. (2010) Numerical models for the seismic assessment of an old masonry tower. *Engineering Structures*, **32**(5), 1466-1478.
7. Page, A.W. (1978) Finite element model for masonry. *Journal of the Structural Division*, **104**(8), 1267-1285.
8. Lourenço, P.B., Rots, J.G., and Feenstra, P.H. (1995) A tensile "Rankine" type orthotropic model for masonry. *Computer Methods in Structural Masonry*, **3**, 167-176.

9. Lourenço, P.B. (1996) *Computational Strategies for Masonry Structures*. Ph.D. Thesis, Delft University of Technology, Delft, The Netherlands.

10. Tahghighi, H. and Rabiee, M. (2015) Nonlinear soil-structure interaction effects on building frames: a discussion on the seismic codes. *Journal of Seismology and Earthquake Engineering*, **17**(2), 141-151.

11. Tahghighi, H. and Mohmmadi, A. (2020) Numerical evaluation of soil-structure interaction effects on the seismic performance and vulnerability of reinforced concrete buildings. *Intrenational Journal of Geomechanics*, **20**(6), 04020072. DOI: 10.1061/(ASCE)GM.1943-5622.0001651.

12. Tahghighi, H. and Rabiee, M. (2017) Influence of foundation flexibility on the seismic response of low to-mid-rise moment resisting frame buildings. *Scientia Iranica*, **24**(3), 979-992.

13. Systemes, D. (2019) *SolidWorks (Version 2019): Dassault Systemes*.

14. Systemes, D. (2014) *ABAQUS (Version 6.14): Dassault Systemes*.

15. Golabchi, M. and Javani Dizaji, A. (2018) *Iranian Architecture Technology*. University of Tehran Press, Tehran , Iran.

16. Ambraseys, N.N. and Melville, C.P. (1982) *A History of Persian Earthquake*. Cambridge University Press.

17. Google (Cartographer) (2019a) Location of Bazaar. Retrieved from https://shorturl.at/bkBKR

18. Google (Cartographer) (2019b) Location of Iran. Retrieved from https://shorturl.at/qtvLW.17.

19. NTC (2008) *Technical Standards for Construction*. Ministry of Infrastructure and Transport, Italy.

20. Degli Abbati, S., D'Altri, A.M., Ottonelli, D., Castellazzi, G., Cattari, S., de Miranda, S., and Lagomarsino, S. (2019) Seismic assessment of interacting structural units in complex historic masonry constructions by nonlinear static analyses. *Computers & Structures*, **213**, 51-71.

21. Valente, M. and Milani, G. (2016) Non-linear dynamic and static analyses on eight historical masonry towers in the North-East of Italy. *Engineering Structures*, **114**, 241-270.

22. Karimi, A.H., Karimi, M.S., Kheyroddin, A., and Amirshahkarami, A. (2016) Experimental and numerical study on seismic behavior of an infilled masonry wall compared to an arched masonry wall. *Structures*, **8**, 144-153.

23. Karimi, A.H., Karimi, M.S., Kheyroddin, A., and Amirshahkarami, A. (2017) Nonlinear modeling of unreinforced masonry wall under in-plane load and investigation of the effect of various parameters. *Journal of Structural and Construction Engineering*, **3**(4), 21-34.

24. Jin, Y.-F., Zhu, B.-Q., Yin, Z.-Y., and Zhang, D.-M. (2019) Three-dimensional numerical analysis of the interaction of two crossing tunnels in soft clay. *Underground Space*, **4**(4), 310-327.

25. Yang, X., Yang, G., and Yu, T. (2012) Comparison of strength reduction method for slope stability analysis based on ABAQUS FEM and FLAC3d FDM. *Applied Mechanics and Materials*.

26. de Silva, F., Ceroni, F., Sica, S., and Silvestri, F. (2018) Non-linear analysis of the Carmine bell tower under seismic actions accounting for soil-foundation-structure interaction. *Bulletin of Earthquake Engineering*, **16**(7), 2775-2808.

27. Ghadimi Chermahini, A. and Tahghighi, H. (2019) Numerical finite element analysis of underground tunnel crossing an active reverse fault: a case study on the Sabzkouh segmental tunnel. *Geomechanics and Geoengineering*, **14**(3), 155-166.

28. Soil Mechanics Laboratory (2010) *Geotechnical Investigations Report of Bab al-Huaij Multi-Story Parking Lot*. Final Report, Islamic Azad University, Kashan, Iran.

29. Schneider, C.A., Rasband, W.S., and Eliceiri, K.W. (2012) NIH Image to ImageJ: 25 years of image analysis. *Nature Methods*, **9**(7), 671, DOI:10.3410/f.717951500.793456800.

30. Salih, Y. and Malik, A.S. (2012) Depth and geometry from a single 2d image using triangulation. *2012 IEEE International Conference on Multimedia and Expo Workshops*, Melbourne, VIC, Australia.

31. Ghosh, S. and Wilson, E.L. (1969) Dynamic Stress Analysis of Axi-Symmetric Structures under Arbitrary Loading. California, Berkeley: University of California.

32. Lagomarsino, S. and Cattari, S. (2015) PER PETUATE guidelines for seismic performance-based assessment of cultural heritage masonry structures. *Bulletin of Earthquake Engineering*, **13**(1), 13-47.

33. Castellazzi, G., D'Altri, A.M., de Miranda, S., and Ubertini, F. (2017) An innovative numerical modeling strategy for the structural analysis of historical monumental buildings. *Engineering Structures*, **132**, 229-248.

34. Fajfar, P. (1999) Capacity spectrum method based on inelastic demand spectra. *Earthquake Engineering and Structural Dynamics*, **28**(9), 979-993.

35. FEMA 440 (2005) *Improvement of Nonlinear Static Seismic Analysis Procedures*. Prepared by Applied Technology Council for Federal Emergency Management Agency, Washington DC, USA.

36. Standard No. 2800 (2014) *Iranian Code of Practice for Seismic Resistance Design of Buildings*. 4th Edn., Ministry of Road, Housing and Urban Development, Tehran, Iran.